Out-of-Step Protection Using State-Plane Trajectories Analysis

Binod Shrestha, *Member, IEEE*, Ramakrishna Gokaraju, *Member, IEEE*, and Mohindar Sachdev, *Life Fellow, IEEE*

***Abstract*—This paper proposes a novel out-of-step protection technique using the state-plane representation of the generator speed and power angle. The critical clearing angle is computed using the principle that the total energy of the system at the instant the fault is cleared should be equal to the maximum potential energy of the system. The critical clearing time corresponding to the value of critical clearing angle is obtained directly using the time calibration of the relative speed versus power-angle solution curve. The simultaneous calculation of the critical clearing angle and the time make the proposed approach much faster than the two-blinder scheme. The proposed state-plane prediction scheme is used to detect the first swing out-of-step condition in a two-area test system using system-wide information. The two generators are represented with a single-machine infinite bus equivalent system, and the state-plane algorithm is applied to the reduced equivalent. Electromagnetic transient simulations are carried out using PSCAD/EMTDC™ to test the proposed algorithm in the two-area test systems. The simulation studies show that the proposed method is computationally efficient and accurate. The technique also does not require any offline studies.**

***Index Terms*—Out-of-step protection, state plane, transient stability.**

I. Introduction

SEVERAL methods are proposed in the literature to predict out-of-step conditions in a power system. The methods are briefly reviewed below.

One of the conventional techniques reported in [1] and [2] is based on the rate of change of impedance. Setting the blinders and determining a pre-set delay are two of the major tasks in this technique. References [2] and [3] describe techniques to set these blinders where the settings are system specific, depend on system loading conditions and are only applicable up to a two-machine system. Setting blinders require extensive system stability studies, and a relay design using blinders to work for all possible system conditions is difficult.

An out-of-step relaying scheme with rate of change of apparent resistance augmentation is proposed in [4]. The relay characteristic is a modified version of the blinder scheme where the rate of change of apparent impedance is replaced with the apparent resistance augmented with the rate of change of apparent resistance and relay characteristic is defined in an R-Rdot plane. The scheme also requires extensive simulation studies under various contingency conditions to set the relay characteristics.

The swing center voltage (SCV) technique discussed in [1] is also an option for out-of-step protection. The disadvantage is that the detection is usually made at a voltage angle separation close to 180°.

Out-of-step detection schemes using transient energy calculation are also proposed in the literature. Reference [5] implements Lyapunov's direct method to predict the out-of-step condition of a generator using local substation measurements. Moreover, the technique does not provide critical clearing time (CCT) information, which is an important piece of information for relaying and stability study purposes.

The equal area criterion (EAC) is popularly used as a transient stability analysis' tool. The approach is directly applicable to a single machine infinite bus system [6]. The technique has been extended to a multi-machine system by Pavella *et al.* [7]. The technique is called an extended EAC (EEAC). Based on the EEAC, an adaptive out-of-step relay was developed by Phadke *et al.* [8]. The relay was implemented on the intertie between the states of Georgia and Florida in the U.S. in October 1993 and was operational until January 1995. The out-of-step detection using EAC is simple and well established; however, EAC-based techniques cannot provide the critical clearing angle (CCA) and CCT for the fault simultaneously. It requires step-by-step integration techniques to calculate CCT.

Reference [9] proposed an out-of-step protection scheme using fuzzy logic and [10] proposed a technique using a neural network. Rajapakse *et al.* [11] proposed a rotor-angle instability prediction technique using fuzzy C-means clustering algorithm and support vector machine. The algorithms work well only if they are sufficiently trained and the training signals are appropriately identified.

Reference [12] proposed an out-of-step detection technique using frequency deviation of voltage method. The technique estimates the frequency using voltage angle calculated at the local bus. Further the angular acceleration is calculated using the calculated frequency. The instability is detected when the frequency measured at the point, where acceleration changes its sign from negative to positive, is greater than zero. Otherwise, the system will be stable. The detection is based on electrical voltage signal which can change very rapidly and may result in false tripping during switching transients. The method is based on local measurements, and a system-wide protection using the technique has not been reported so far.

Reference [13] proposed an instability detection method using a transient instability index, defined as μ. The μ index is calculated based on the generator angle, speed and their rate

Manuscript received July 01, 2012; revised November 27, 2012; accepted January 09, 2013. Date of publication February 26, 2013; date of current version March 21, 2013. Paper no. TPWRD-00683-2012.

The authors are with the University of Saskatchewan, Saskatoon, SK S7N 5A9 Canada (e-mail: bis094@campus.usask.ca; rama.krishna@usask.ca; sachdev@sasktel.net).

Color versions of one or more of the figures in this paper are available online at http://ieeexplore.ieee.org.

Digital Object Identifier 10.1109/TPWRD.2013.2245684

of change to identify the characteristics concave and convex nature of a surface on which postfault trajectories lie. If the μ index is less than 1, it represents a convex surface and the system is detected to be unstable. If the index is greater than 1, it represents concave surface and the system is detected to be stable.

Reference [14] proposed an out-of-step detection technique using energy equilibrium in time domain. In [14], the classical equal area conditions in the power-angle domain were mapped to the time domain, and the out-of-step conditions were identified graphically by point-by-point analysis directly in the time domain. The accelerating and decelerating area in a power vs time curve is calculated. If the decelerating area becomes equal to the accelerating area during the transient, the system becomes stable. If the accelerating area is greater than decelerating area, the system becomes unstable. The disadvantage of this technique is that the unstable condition is again detected close to 180° and, hence, the opening of the breakers have to be delayed until the angle of separation between the two side voltages becomes a favorable angle (to reduce the restriking voltage level).

State plane analysis methods are widely used in the control systems literature for analyzing the dynamics of second-order systems using phase portraits [15]. The classical power systems literature [16]–[18] describe various solutions methodologies for the Lyapunov's stability criteria using phase portraits, which could be called the state-plane methods.

This paper proposes a new out-of-step prediction algorithm using state-plane plot of speed vs power angle. A two area system, after disturbance, is represented with a single-machine infinite bus (SMIB) equivalent system. The state-plane analysis (SPA) algorithm is applied to the SMIB equivalent where, the dynamic states of the SMIB equivalent during the disturbance and, after the disturbance are represented using state-plane plot. The plot was used to find whether the system is going to be stable or unstable. The CCA of the equivalent system is found when the total energy of the system at the instant the fault is cleared becomes equal to the maximum potential energy of the system. The time corresponding to this delta value (i.e., CCT) is found directly from the omega vs delta curve unlike the equal area criterion approach. Thus, the CCA and CCT, which have been obtained simultaneously, are used to predict a stable or out-of-step condition in power system. The proposed algorithm has been tested in a two area test system using the electromagnetic transient simulations tool, PSCAD/EMTDC™[1]. Electromagnetic simulations have been used instead of the steady-state stability programs (phasor solution) since the electromagnetic-transient (EMT) simulations provide more detail and closer resemblance to an actual power system. The simulation studies show that the proposed method is faster, computationally efficient, and accurate.

Section II describes the angular separation and SMIB equivalencing procedure. Section III describes the state-plane method. Section IV describes out-of-step prediction using the state-plane analysis method. Section V gives the case studies and Section VI gives the final conclusions.

[1]PSCAD/EMTDC is a registered trademark of Manitoba HVDC Centre, Winnipeg, MB, Canada.

II. SMIB Equivalent

A. Identifying Angular Separation Between Two Areas

The angular separation of the generators is identified in real time using the generator swing curves. It uses the principles of identifying coherent group of generators as explained in [19] and [20]. The coherent groups are found from the generator rotor angles and the bus voltage phase angle changes which have the most consistently similar pattern over all the inter-area modes. For the power system configuration (consisting of two areas interconnected through a tie-line), the generators in each area normally form a coherent group and participate in the inter-area oscillations. In real time, the angular separation is identified by measuring the difference in generator bus voltage angles of the two areas and is compared with the threshold angle during the postfault condition.

Therefore, the separation between the generators is identified using the criterion given by

$$\Delta\theta_i - \Delta\theta_r < \epsilon \tag{1}$$

where ϵ is the specified tolerance in degrees, i represents the area 1 machine, and r represents the reference generator (area 2 machine). A tolerance of 5° is selected for this study. When the angular separation between the two areas exceeds 5°, the relay is triggered to check for instability (i.e., stable or unstable swing).

B. SMIB Equivalent

The two-machine system can be reduced to an SMIB equivalent system with single machine parameters δ, ω, M, P_m, and P_e as given by (9). The procedure is described in [7]. The proposed algorithm is implemented using the swing equation of the SMIB equivalent to determine the out-of-step condition in the two-area system.

With the classical model, the generator dynamics are described by (2) [7]

$$\dot{\delta_i} = \omega_i, \quad M_i \frac{d\omega_i}{dt} = P_{mi} - P_{ei} \tag{2}$$

where

$$P_{ei} = E_i^2 Y_{ii} \cos\theta_{ii} + \sum_{\substack{j=1 \\ j\neq 1}}^{n} E_i E_j Y_{ij} \cos(\delta_i - \delta_j - \theta_{ij}) \tag{3}$$

M_i	inertia constant of the ith generator;
δ_i	internal voltage angle of the ith generator;
ω_i	rotor speed of the ith generator;
P_{mi}/P_{ei}	mechanical input/electrical output power of the ith generator;
E_i, E_j	voltage behind transient reactance;
Y	admittance matrix reduced at the internal generator node;
$Y_{ij}(\theta_{ij})$	modulus (argument) of the ijth element of Y.

Fig. 1. Two-machine representation.

Using the assumption made by [7] that the disturbed multimachine system separates in two groups, let us define the two groups of machines as an Area A and Area B as shown in Fig. 1.

The partial center of angles (PCOA) of Area A and that of Area B are given by

$$\delta_a = \sum_{i\in A} \frac{M_i\delta_i}{M_a} \tag{4a}$$

$$M_a = \sum_{i\in A} M_i \tag{4b}$$

$$\delta_b = \sum_{j\in B} \frac{M_j\delta_j}{M_b} \tag{4c}$$

$$M_b = \sum_{j\in B} M_j \tag{4d}$$

where δ_a is the COA of the generators in Area A, M_a is the sum of the inertia constants of the generators in Area A, δ_b is the COA of the generators in Area B, and M_b is the sum of the inertia constants of the generators in Area B. The COA of a group is assumed to be equal to the rotor angles of the generators in that group, i.e.,

$$\delta_a = \delta_i \quad \forall\, i\epsilon A \tag{5a}$$

$$\delta_b = \delta_j \quad \forall\, j\epsilon B. \tag{5b}$$

Using the above formulations, two groups of generators can be transformed into two-machine systems running in their own PCOA. The motion of PCOAs of Group A and B in the two-machine system are described by.

$$M_a\ddot{\delta_a} = \sum_{i\in A}(P_{mi} - P_{ei}) \tag{6a}$$

$$M_b\ddot{\delta_b} = \sum_{j\in S}(P_{mj} - P_{ej}) \tag{6b}$$

where

$$P_{ei} = E_i^2 Y_{ii}\cos\theta_{ii} + E_iE_jY_{ij}\cos(\delta_a - \delta_b - \theta_{ij}) + \sum_{\substack{i\in A\\ i\neq j}} E_iE_jY_{ij}\cos\theta_{ij} \tag{7}$$

$$P_{ej} = E_j^2 Y_{jj}\cos\theta_{jj} + E_jE_iY_{ji}\cos(\delta_b - \delta_a - \theta_{ji}) + \sum_{\substack{j\in B\\ j\neq i}} E_jE_iY_{ji}\cos\theta_{ji}. \tag{8}$$

The two-machine system can further be reduced to an SMIB equivalent system with a single-machine parameter δ, ω, M, P_m, P_e. The motion of the resulting SMIB equivalent system can be described using

$$M\ddot{\delta} = P_m - (P_c + P_{\max}\sin(\delta - \gamma)) \tag{9}$$

where

$$\delta = \delta_b - \delta_a \tag{10a}$$

$$M = \frac{M_bM_a}{M_T} \tag{10b}$$

$$M_T = \sum_{i=1}^{n} M_i \tag{10c}$$

$$P_m = (M_a\sum_{j\in B} P_{mj} - M_b\sum_{i\in A} P_{mi}){M_T}^{-1} \tag{10d}$$

$$P_c = (M_a\sum_{j,k\in B} E_jE_kG_{jk} - M_b\sum_{i,l\in A} E_iE_lG_{il}){M_T}^{-1} \tag{10e}$$

$$P_{\max} = \sqrt{C^2 + D^2} \tag{10f}$$

$$\gamma = -\arctan\left(\frac{C}{D}\right) \tag{10g}$$

$$C = (M_a - M_b){M_T}^{-1}\sum_{i\in A, j\in B} E_iE_jG_{ij} \tag{10h}$$

$$D = \sum_{i\in A, j\in B} E_iE_jB_{ij} \tag{10i}$$

where δ and M are the rotor angle and inertia constant of the SMIB equivalent, respectively; M_T is the sum of the inertia constants of n generators; n represents the total number of generators; P_m and P_e are the mechanical input power and electrical output power of SMIB equivalent, respectively; and B and G are the susceptance and conductance of the network, respectively.

III. State-Plane Analysis

Consider that a power system is described with the following second-order differential equation

$$\ddot{\delta} = f(\delta, \dot{\delta}). \tag{11}$$

Let us define the state variables as

$$x_1 = \delta$$
$$x_2 = \dot{\delta}. \tag{12}$$

Equation (11) can now be represented with a set of first-order differential equations

$$\dot{x_1} = x_2$$
$$\dot{x_2} = f(x_1, x_2). \tag{13}$$

The plane, with coordinates x_1 and x_2, is called the state plane. The solution of (13) with respect to time could be represented as a curve in state plane (state-plane trajectory). If one knows the initial states of the system, the dynamics followed by the power system during fault could be easily predicted using the state-plane trajectory. Also, the state-plane trajectories for different initial states could be represented in a graphical fashion

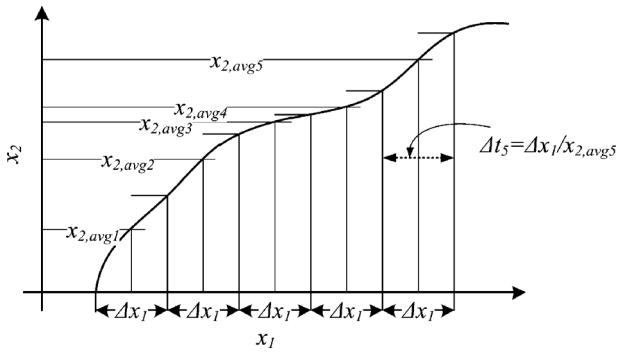

Fig. 2. Time calculation from the state-plane trajectory.

to analyze the power system behavior for various types of contingencies in a power system.

Eliminating time from (13) gives

$$\frac{dx_2}{dx_1} = \frac{f(x_1, x_2)}{x_2}. \tag{14}$$

Equation (14) can be written as

$$\frac{dx_2}{dx_1} = \frac{Q(x_1, x_2)}{P(x_1, x_2)}. \tag{15}$$

The point for which the system is going to be at rest (i.e., $P(x_{1s}, x_{2s}) = 0$ and $Q(x_{1s}, x_{2s}) = 0$) is a singular point. The system will continuously stay at a singular point if it is left undisturbed. Singular points hence represent points of equilibrium. The determination of singular points represent an essential step in the process of plotting the state-plane trajectories. The stable and unstable equilibrium points are called the vortex and saddle point, respectively.

A. Determining Time From Trajectories

A state-plane trajectory contains time information implicitly. The time information can be extracted from the trajectory by using a simple procedure as explained below. The state variable x_1 can be evenly or unevenly divided into small intervals. For each small increment of x_1, an average increment in x_2 can be calculated and, hence, the corresponding small increment in time can be calculated using (16a). In Fig. 2, x_1 is evenly divided into small intervals Δx_1. The small increment in time Δt for Δx_1 and $x_{2,avg}$ corresponding to the ith interval is given by (16b)

$$dt = \frac{dx_1}{x_2} \tag{16a}$$

$$\Delta t_i = \frac{\Delta x_1}{x_{2,avgi}}. \tag{16b}$$

The time for each point of interval is now calculated by cumulatively adding the incremental time for each interval

$$t(i) = t(i-1) + \Delta t_i. \tag{17}$$

B. State-Plane Representation of Swing Equation

Given the swing equation

$$M\frac{d^2\delta}{dt^2} = P_m - P_{\max}\sin\delta. \tag{18}$$

Equation (18) could be modified as

$$\frac{d^2\delta}{dT^2} = P - \sin\delta \tag{19}$$

where $P = P_m/P_{\max}$, $T = t\sqrt{\pi * P_{\max}/180 * M}$ and $P_{\max}$ is the maximum electrical power value that could flow through the lines. State-space representation of (19) is given by

$$\dot{\delta} = \omega \tag{20a}$$

$$\dot{\omega} = P - \sin\delta \tag{20b}$$

where δ and ω are two state variables and ω represents the speed of the machine with respect to the synchronous speed. The two state variables give the current dynamic state of the machine. During the transient condition, the machine starts oscillating because of the change in P in (19). As a result, the state variables exhibit oscillatory behavior. The dynamic motion of the machine is hence represented by the change in state variables of the system, which can be demonstrated by plotting state variables ω versus δ in a state plane. The path followed by state variable ω in the state plane with respect to δ gives important information about stability of the synchronous machines. Angle δ gives the position of the rotor, and the speed ω represents the energy associated with the machine. Equation (20) can also be written as

$$\frac{d\omega}{d\delta} = \frac{P - \sin\delta}{\omega}. \tag{21}$$

The singular points of the system could be found out by equating the numerator and denominator of the right-hand side of (21) to zero (i.e., $P - \sin\delta = 0$ and $\omega = 0$). The singular points will be $(\sin^{-1} P, 0)$ and $(\pi - \sin^{-1} P, 0)$. The stability of the system around these points could be obtained by analyzing the eigenvalues of the system (Lyapunov's indirect method) [15]. Using this analysis, the first point is found to be a stable equilibrium point, and the second point is obtained as an unstable equilibrium point. Equation (21) can be rearranged so that the same variables appear on one side

$$\omega d\omega = (P - \sin\delta)d\delta. \tag{22}$$

Integrating both sides of (22) gives

$$\underbrace{\frac{\omega^2}{2}} + \underbrace{\int_0^{\delta}(\sin\delta - P)d\delta} = 0 \tag{23}$$

where the first term in the left-hand side of (23) represents kinetic energy, and the second term represents potential energy of the machine. Since the kinetic energy is zero at the singular point, it gives maximum or minimum of potential energy.

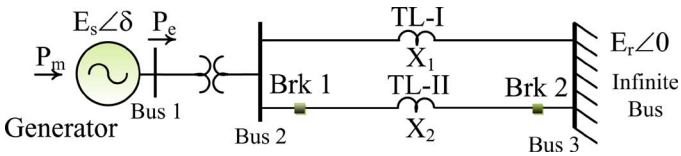

Fig. 3. SMIB equivalent system.

Section IV describes state-plane trajectories during different transient states (prefault, during fault, and postfault) of a power system.

C. State-Plane Trajectory Plots

Consider an SMIB equivalent system as shown in Fig. 3. The SMIB system parameters are given in the Appendix.

Under normal conditions, the system operates at a stable equilibrium point, referred to as *prefault condition*, delivering constant electrical power. The initial state of the generator is (0.738 rad, 0 rad/s). A three-phase fault is applied at the middle of transmission line II, referred to as *during-fault condition*, and the fault is cleared by opening the breakers Brk1 and Brk2 at the two ends of the line, referred to as the *postfault condition*. The state-plane trajectories are plotted for the aforementioned conditions with the initial points, varied from -2.5 to 4.5, for illustration purpose. The plots are shown in Figs. 4–6, respectively. In the figures, the three different lines are denoted as follows.

- Solid blue lines are isoclines plotted for different values of $d\omega/d\delta$ varying from -5 to 5 with an equal interval of 0.5. All isoclines go through the singular points and, hence, the intersections of them give the singular points.
- Solid black lines are the state-plane trajectories.
- Dotted red line is critical trajectory known as separatrix.

1) ***Prefault Condition:*** For the prefault system, the value of P is 0.673 p.u. ($P_{\max}$ for the prefault condition is 1.3370 p.u.). Fig. 4 shows the various possible paths that the machine can follow during the prefault condition. Since the machine is operating at (0.738 rad, 0 rad/s), which is the vortex of the system, the machine stays stable. The trajectories near the vortex are bounded around it and the region is a stable region. The trajectories around the saddle are unbounded (where ω increases as δ increases) and the region is called an unstable region. These two regions are separated by a separatrix.
2) ***During-fault condition:*** For the three-phase fault, the value of P is 1.20 p.u. ($P_{\max} = 0.7480$ p.u.). Fig. 5 shows the state-plane trajectories for a three-phase fault. As can be seen from the trajectories, there are no singular points.
3) ***Postfault condition:*** The fault is cleared by removing the faulted line from the system. The P value becomes 0.95 p.u. ($P_{\max} = 1.1024$ p.u.) and the postfault trajectories are shown in Fig. 6.

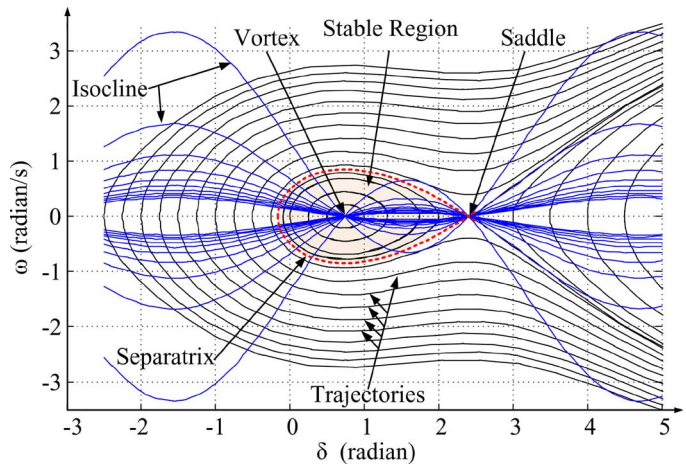

Fig. 4. State-plane trajectories of an SMIB for a prefault condition.

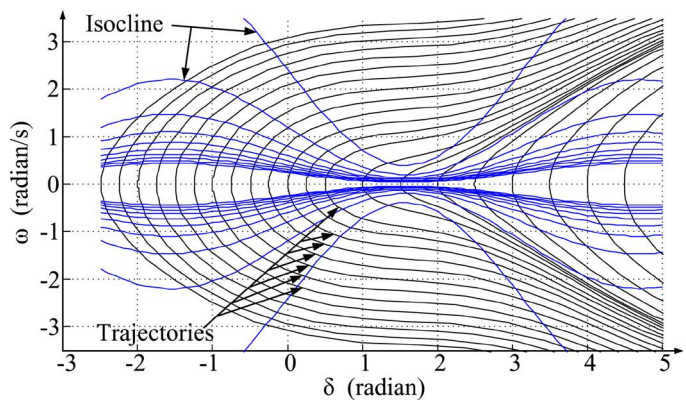

Fig. 5. State plane trajectories of an SMIB for a during-fault condition.

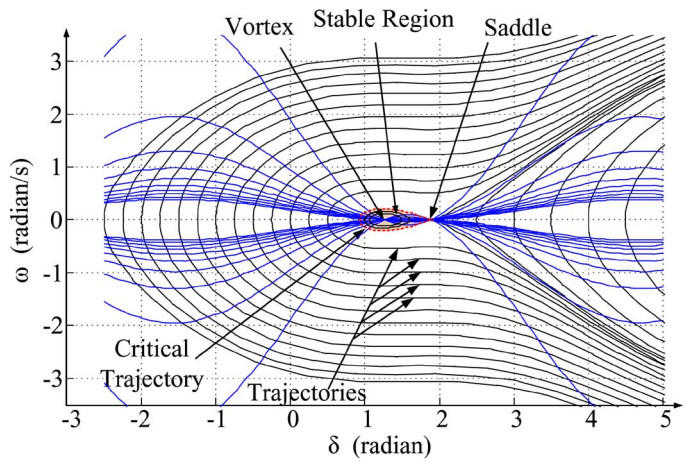

Fig. 6. State-plane trajectories of an SMIB for a postfault condition.

IV. Out-of-Step Prediction (State Plane Analysis)

The algorithm calculates the system's critical clearing angle(δ_{cr}) and the critical clearing time (t_{cr}) simultaneously using the state-plane plot of during-fault and postfault conditions. The t_{cr} calculated is compared with the fault clearing time (t_{cl}) to make the decision. The algorithm consists of four distinct steps:

1) Step—I Find State Plane Plot During Disturbance: Suppose the initial state is $(\delta_0, 0)$, (21) can be used to calculate ω for

TABLE I
CALCULATE DURING-FAULT TRAJECTORY AND TIME SCALE

δ (rad)	ω_1 (rad/s)	$\Delta\delta$ (rad)	ω_{1avg} (rad/s)	ΔT (s)	Δt (s)	t (s)
0.7711	0.0000					0.00
0.8025	0.2466	0.0314	0.1233	0.2548	0.0462	0.0462
0.8339	0.3467	0.0314	0.2966	0.1059	0.0192	0.0653
0.8653	0.4223	0.0314	0.3845	0.0817	0.0148	0.0801
0.8968	0.4849	0.0314	0.4536	0.0693	0.0125	0.0927
0.9282	0.5392	0.0314	0.5121	0.0614	0.0111	0.1038
0.9596	0.5875	0.0314	0.5633	0.0558	0.0101	0.1139
0.9910	0.6312	0.0314	0.6093	0.0516	0.0093	0.1232
1.0224	0.6713	0.0314	0.6512	0.0482	0.0087	0.1320
1.0538	0.7083	0.0314	0.6898	0.0455	0.0082	0.1402
1.0853	0.7429	0.0314	0.7256	0.0433	0.0078	0.1480
1.1167	0.7754	0.0314	0.7591	0.0414	0.0075	0.1555
1.1481	0.8060	0.0314	0.7907	0.0397	0.0072	0.1627
1.1795	0.8350	0.0314	0.8205	0.0383	0.0069	0.1697
1.2109	0.8626	0.0314	0.8488	0.0370	0.0067	0.1764
1.2423	0.8889	0.0314	0.8757	0.0359	0.0065	0.1829
1.2737	0.9142	0.0314	0.9015	0.0348	0.0063	0.1892
1.3052	0.9384	0.0314	0.9263	0.0339	0.0061	0.1953

incremental values of δ. The derived expression for ω_1 is given by (24). It gives the values of ω_1 versus δ during the disturbance

$$\omega_1 = \pm\sqrt{2(P_1(\delta-\delta_0)+\cos\delta-\cos\delta_0)} \tag{24}$$

where $\omega_1 = d\delta/dT_1$ is the speed of the machine, and P_1 is the value of P for the during-fault condition.

2) Step—II Calculate Time Scale Values: The time scale values for (Step—I) are calculated using the method explained in Section III-A. The calculated time would be the time T_1 from which the exact time is calculated using

$$t(i) = T_1(i) \times \mathrm{TF}_1 \tag{25}$$

where

$$\mathrm{TF}_1 = \sqrt{\frac{180 * M}{\pi * P_{\mathrm{maxdf}}}} \tag{26}$$

where P_{maxdf} refers to maximum power that can be transferred for a during-fault condition.

The SMIB equivalent system as shown in Fig. 3 is used to illustrate the algorithm. A three-phase fault is applied on TL-II at (1/4)th distance from bus 2. The test case is named as "E." The initial generator bus voltage angle (δ_t) is 30° and the initial voltage angle behind transient reactance is 44.1803° (0.7711 radian). The mechanical input power is 0.9486 p.u. For the faulted network condition, the power-angle characteristic is obtained using the standard Y_{BUS} network reduction technique [6]. The $P_e - \delta$ curve obtained is $0.5661\sin\delta$. The ω_1 and time (t) values calculated for the during-fault condition are given in Table I.

3) Step—III Find Critical Trajectory (Separatrix) for Postfault Condition: The postfault power-angle characteristic is predicted using the postfault network condition. The power-angle characteristic for the test case E is $1.1024\sin\delta$. The postfault swing equation is therefore given by (27)

$$\frac{d^2\delta}{dT_2^2} = P_2 - \sin\delta \tag{27}$$

$$\frac{d^2\delta}{dT_2^2} = 0.8604 - \sin\delta. \tag{28}$$

The above equation can be put in the form

$$\frac{d\omega_2}{d\delta} = \frac{0.8604-\sin\delta}{\omega_2} \tag{29}$$

where $\omega_2 = d\delta/dT_2$ and P_2 are the value of P for the postfault condition.

The singularities for (29) are obtained by equating the numerator and denominator to zero. The singular points are located at (1.036,0) and (2.105,0). For the first singular point (1.036,0), define translated states as $\widetilde{\delta} = \delta - 1.036$ and $\widetilde{\omega_2} = \omega_2$. The corresponding state equation becomes

$$\frac{d\widetilde{\omega_2}}{d\widetilde{\delta}} = \frac{0.8604-\sin(\widetilde{\delta}+1.036)}{\omega_2} \tag{30}$$

which could also be written as

$$\begin{bmatrix} \dot{\widetilde{\delta}} \\ \dot{\widetilde{\omega_2}} \end{bmatrix} = \begin{bmatrix} \omega_2 \\ 0.8604-\sin(\widetilde{\delta}+1.036) \end{bmatrix}. \tag{31}$$

Equation (31) is linearized around (0,0). The linearized system is given by

$$\begin{bmatrix} \dot{\widetilde{\delta}} \\ \dot{\widetilde{\omega_2}} \end{bmatrix} = \begin{bmatrix} 0 & 1 \\ -0.51 & 0 \end{bmatrix} \begin{bmatrix} \widetilde{\delta} \\ \omega_2 \end{bmatrix}. \tag{32}$$

The eigenvalues of the system are $\pm 0.712i$, which results in an oscillatory system with zero damping. This singular point corresponds to a vortex point. Following a similar procedure for the singular point (2.105,0), the eigenvalues obtained are ± 0.712. This will result in an unstable system and, hence, the singular point is a saddle point.

Equation (23) for the postfault condition can be written as

$$\frac{\omega_2^2}{2} + \int_0^{\delta} (\sin\delta - P_2)\, d\delta = 0. \tag{33}$$

Equation (33) can be written as

$$\frac{\omega_{2cl}^2}{2} + \int_0^{\delta_{cl}} (\sin\delta - P_2)\, d\delta = 0 \tag{34}$$

where δ_{cl} is the value of δ and ω_{2cl} is the speed of the machine when the fault is cleared. ω_{2cl} is given by

$$\omega_{2cl} = \left(\frac{d\delta}{dT_2}\right)_{T_2=0} = \frac{dT_1}{dT_2}\frac{d\delta}{dT_1} = \left(\frac{\mathrm{TF}_1}{\mathrm{TF}_2}\right)\omega_1 \tag{35}$$

where TF_1 is given by (26) and

$$\mathrm{TF}_2 = \sqrt{\frac{180 * M}{\pi * P_{\mathrm{maxaf}}}} \tag{36}$$

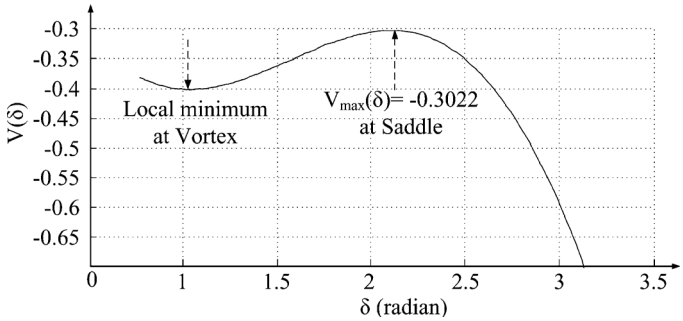

Fig. 7. Potential energy plot for test case E.

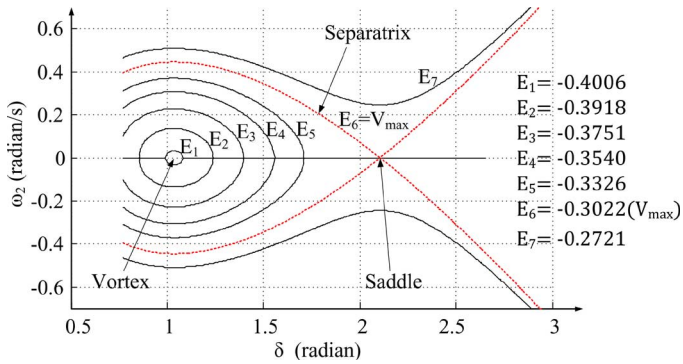

Fig. 8. State- plane trajectories of SMIB for postfault condition for different values of E.

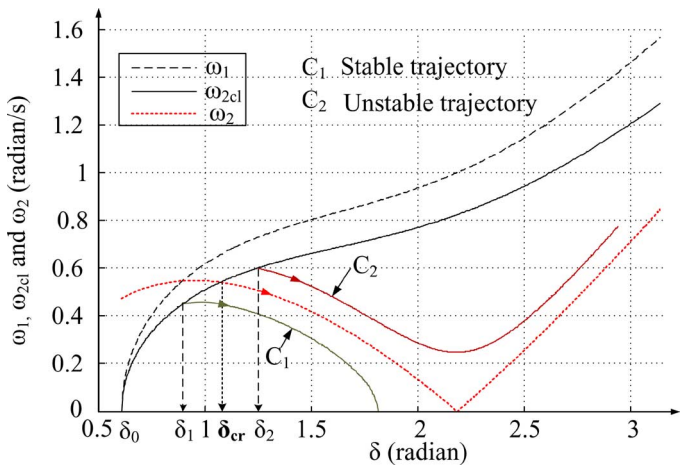

Fig. 9. Finding the critical clearing angle.

where P_{maxaf} is the maximum possible power transfer for the postfault condition. As discussed in Section III-B, the potential energy $(V(\delta) = \int_0^{\delta} (\sin\delta - P_2)\, d\delta)$ of the machine will have a maximum and a minimum at the singular points. It can be seen by setting the first derivative of potential energy $(dV/d\delta)$ to zero which means $(\sin\delta - P_2 = 0)$. The second derivative of $V(\delta)$ is $\cos\delta$. For singular point $(\sin^{-1} P_2, 0)$, the second derivative is positive and, therefore, it results in a minimum, and for singular point $(\pi - \sin^{-1} P_2, 0)$, it is negative, resulting in a maximum. Fig. 7 shows the plot of potential energy for the test case E.

The minimum potential energy occurs at the vortex point and the maximum potential energy $(V_{\max})$ occurs at the saddle point. If the total energy of the machine (i.e., sum of kinetic energy gained during the fault condition and potential energy gained for the postfault condition) is less than $V_{\max}$ at the moment when the disturbance is cleared, the machine becomes stable. Otherwise, it becomes unstable. Equation (33) can be written in the form given by (37). From (37), the state ω_2 can be calculated, which is given by

$$\frac{\omega_2^2}{2} + V(\delta) = E \tag{37}$$

$$\omega_2 = \sqrt{2(E - V(\delta))}. \tag{38}$$

For different values of total energy E_i (where $i = 1, 2, \ldots, 7$), state-plane plots for ω_2 are shown in Fig. 8. When the value of E becomes equal to $V_{\max}$, the corresponding trajectory gives the separatrix. For $(i = 1, 2, \ldots, 5)$, E_i is less than $V_{\max}$, which means that the system is stable, and the total energy E_7 is greater than $V_{\max}$, which indicates that the system becomes unstable.

4) Step—IV Find CCA (δ_{cr}) and CCT (t_{cr}): Two approaches could be used for calculating the critical clearing angle of the system and are explained as follows.

1) When the sum of the kinetic energy gained by the machine for the during-fault condition and the potential energy that can be gained by the machine for the after-fault condition is equal to the maximum potential energy $(V_{\max})$, it gives the CCA (δ_{cr}).

$$E = \frac{\omega_{2cl}^2}{2} + \int_0^{\delta_{cr}} (\sin\delta - P_2)\, d\delta = V_{\max}. \tag{39}$$

2) In the state-plane plot shown in Fig. 9, starting from δ_0, ω_{2cl} represents the kinetic energy gained by the machine at the moment when the fault is cleared and the ω_2 is the separatrix which represents the gain in potential energy by the machine after the fault condition. If the fault is cleared at angle δ_1, postfault speed will follow the C_1 curve, which shows stable operation. At the point of intersection of these two plots, the sum of the gain in kinetic energy gained during fault and the potential energy for after the fault condition will be equal. The point of intersection gives the critical clearing point and the corresponding angle will be the CCA (δ_{cr}) as shown in Fig. 9. If the fault is cleared at angle δ_2, postfault speed will follow the C_2 curve (since the speed keeps on increasing, the machine becomes unstable). If the fault is not cleared from the system due to breaker failure, speed will follow the during-fault trajectory (ω_1) and the machine becomes unstable.

The second approach has been adopted here to calculate the CCA. The angle δ, time scale (t), and ω_{2cl} and ω_2 calculated for the test case E are shown in Table II. The point of intersection of ω_{2cl} and ω_2 is found by calculating the absolute difference between ω_{2cl} and ω_2. The minimum difference gives the point of intersection. The critical clearing time (t_{cr}) can now be calculated using the time scale given in Step II. From Table II, the CCA determined is 0.9910 radian and the CCT observed is 0.1232 s. Fig. 10 demonstrates the procedure.

A decision is made based on the following logic: If $t_{cr} < t_{cl}$: **Stable swing**, if $t_{cr} = t_{cl}$: **Critical condition** and if $t_{cr} > t_{cl}$: **Unstable swing**.

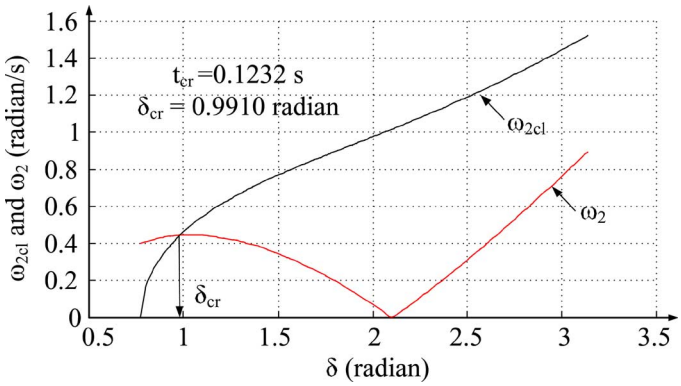

Fig. 10. State-plane trajectories to find CCA and CCT for test case E.

TABLE II
CALCULATION OF CCA AND CCT

Index	δ (radian)	t (s)	ω_{2cl} (radian/s)	ω_2 (radian/s)	abs(ω_{2cl}-ω_2) (radian/s)
1	0.7711	0.0000	0.0000	0.3961	0.3961
2	0.8025	0.0462	0.1767	0.4080	0.2313
3	0.8339	0.0653	0.2485	0.4179	0.1695
4	0.8653	0.0801	0.3026	0.4261	0.1235
5	0.8968	0.0927	0.3475	0.4326	0.0851
6	0.9282	0.1038	0.3864	0.4376	0.0512
7	0.9596	0.1139	0.4210	0.4412	0.0203
8	0.9910	0.1232	0.4523	0.4436	0.0088
9	1.0224	0.1320	0.4810	0.4447	0.0364
10	1.0538	0.1402	0.5076	0.4446	0.0630
11	1.0853	0.1480	0.5324	0.4434	0.0890
12	1.1167	0.1555	0.5556	0.4412	0.1144
13	1.1481	0.1627	0.5776	0.4380	0.1396
14	1.1795	0.1697	0.5983	0.4338	0.1645
15	1.2109	0.1764	0.6181	0.4288	0.1894
16	1.2423	0.1829	0.6370	0.4228	0.2142
17	1.2737	0.1892	0.6551	0.4160	0.2391
18	1.3052	0.1953	0.6725	0.4083	0.2641

The algorithm is summarized in the flowchart shown in Fig. 11.

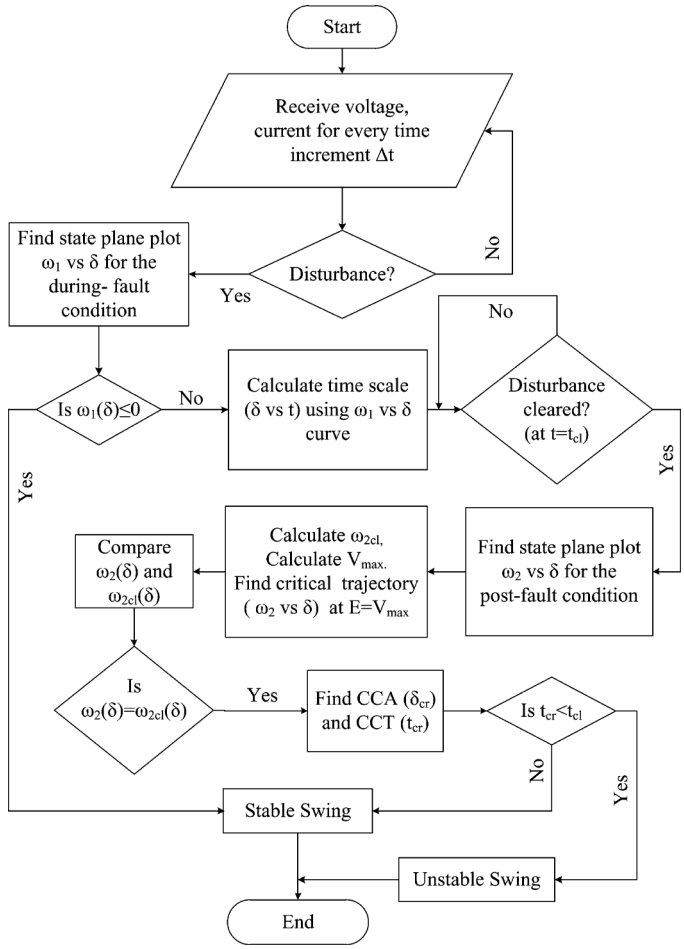

Fig. 11. Flowchart of the proposed state-plane trajectory algorithm.

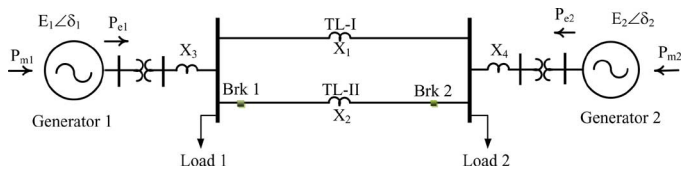

Fig. 12. Two-machine system.

V. CASE STUDIES

A two-area power system model consisting of a machine with finite inertia in each area is considered for the study. Fig. 12 shows the power system configuration. The parameters of generators and transmission lines of the system are given in the Appendix. The identification of groups of machines is performed using coherency analysis. The two-area system can then be transformed into an SMIB equivalent using the procedure explained in Section II-B. State-plane analysis is then performed on the SMIB equivalent system to calculate CCT.

A. Test Cases

The two-area system is tested for various fault durations and two different fault locations. Case 1) a three-phase fault is applied on the transmission line TL-II which is 50 km away from bus 4, and the fault is cleared by opening the faulted transmission line between bus 4 and bus 5. For a fault duration varying from 6 cycle to 20 cycles, stable, unstable, and multiswing unstable cases are observed. Case 2) a three-phase fault is applied on transmission line TL-II, which is 75 km away from bus 4 and is cleared by opening breakers Brk1 and Brk2. Fault duration varies from 8 cycles to 26 cycles to develop stable, unstable, and multiswing unstable cases. In all test cases, the detection time is calculated from the time of fault inception.

1) Stable Swings: For Case 1, a three-phase fault is applied for 6 cycles (0.1 s). Angular separation of the two generator buses is shown in Fig. 13. When the postfault rotors' angles separate more than 5° from the initial postfault value, the relay starts the SMIB equivalent procedure for the two-area system. The system information (i.e., fault location and breaker status during and after fault) is communicated to the relay. The power-angle characteristics for during and postfault predicted by the

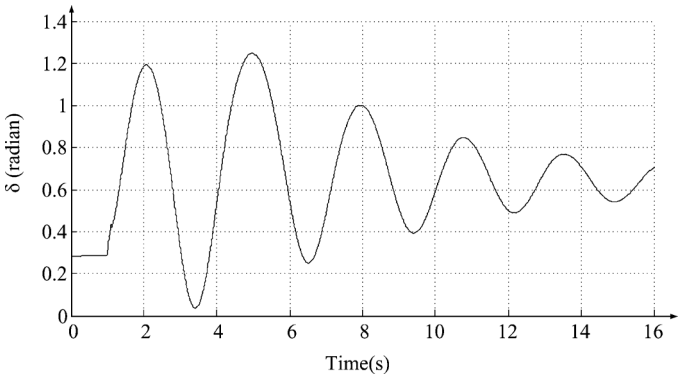

Fig. 13. SMIB equivalent power-angle plot, fault duration of six cycles (Case 1).

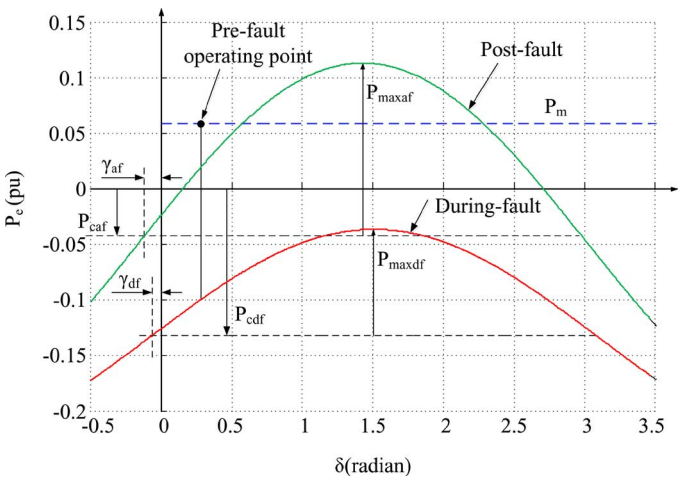

Fig. 14. Power-angle characteristics of the SMIB equivalent (Case 1).

TABLE III
POWER-ANGLE CHARACTERISTICS VALUES FOR CASE 1

During-fault		Post-fault	
$P_{cdf}(pu)$	-0.1318	$P_{caf}(pu)$	-0.0458
$P_{maxdf}(pu)$	0.0954	$P_{maxaf}(pu)$	0.1591
$\gamma_{df}(radian)$	0.0584	$\gamma_{af}(radian)$	0.1383
CCT(s)		0.2704	

relay for Case 1 are shown in Fig. 14. The values for parameters in Fig. 14 are given in Table III.

Using the predicted values of the parameters as shown in Table III, the relay calculates the CCT of the system. Fig. 15 shows the state-plane plot and the time scale generated by the relay to calculate CCT. The CCT calculated for this case is 0.2704 s. Since the fault clearing time (i.e., 0.1 s) is less than the calculated CCT, the swing is detected to be stable and the detection time is 0.2400 s.

2) Unstable Swings: Two unstable cases are discussed here. For case 1, a fault duration of 18 cycles (0.3 s) is used.

When the fault is applied at 1 s and cleared after 18 cycles, the two areas start separating. Fig. 16 shows the rotor-angle separation of the generators. As soon as the angle separation exceeds 5°, the relay starts calculating SMIB equivalent parameters. The parameters calculated for Case 1 will be the same as that shown in Table III. The calculated CCT is 0.2704 s. Since the fault

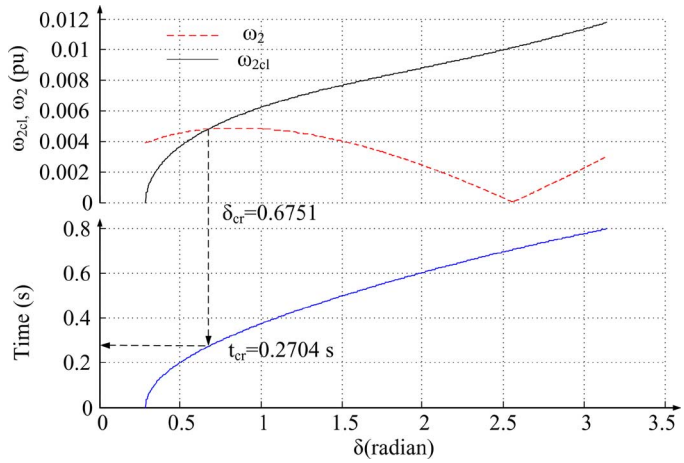

Fig. 15. State-plane and time-scale plots to calculate CCT for Case 1.

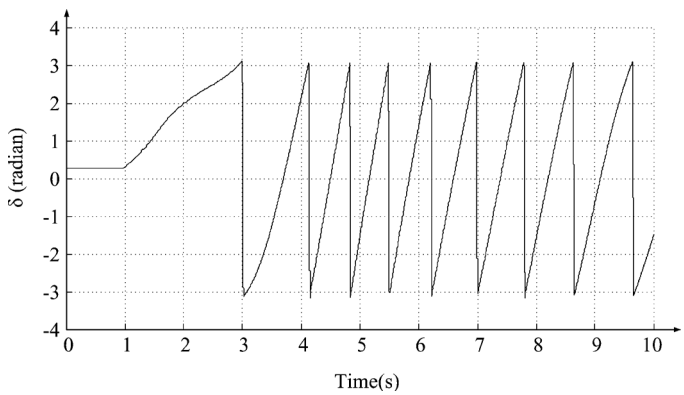

Fig. 16. SMIB equivalent power-angle plot for Case 1, fault duration of 18 cycles.

clearing time (0.3 s) is greater than the calculated CCT, the relay detects the swing as an unstable swing at 0.3700 s.

For Case 2, an unstable case is created by applying a fault for 24 cycles (0.4 s). The two machines oscillate with each other in response to the disturbance as shown in Fig. 17. As soon as the generator bus angles separation exceeds 5° during the postfault period, the relay starts the SMIB equivalent procedure. The power-angle characteristics are again predicted by the relay for during fault and postfault conditions of the network. The values of parameters are given in Table IV.

The CCT calculated using the state-plane analysis (SPA) is 0.3679 s. The fault duration is greater than the CCT; hence, the system becomes unstable. The instability is detected at 0.4700 s. Table V shows the summary of the results for stable and unstable swings detected using the proposed technique based on SPA.

B. Comparison With the Two Blinder Method

A distance relay with a two blinder scheme is placed at transmission line TL-I near bus 4. The relay protects 80% of the line. The inner blinder is set at 0.85 p.u. and the outer blinder is set at 4 p.u. The power swing blocking time delay is taken as 2.5 cycles as recommended by [1].

For Case 1 and the fault applied for 6 cycles, the apparent impedance seen by the distance relay is shown in Fig. 18. Since the impedance locus does not enter the inner blinder, the swing

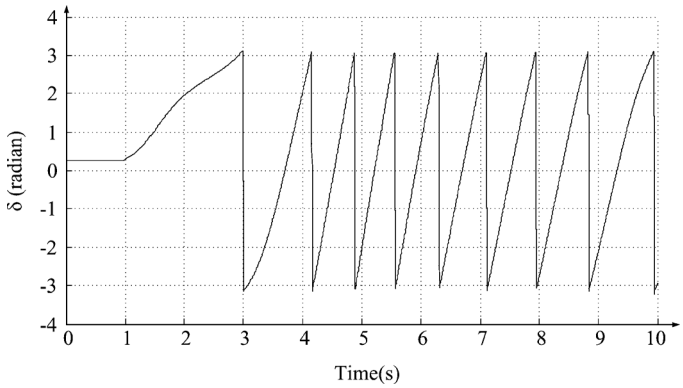

Fig. 17. SMIB equivalent power-angle plot for Case 2, with a fault duration of 24 cycles.

TABLE IV
POWER-ANGLE CHARACTERISTICS VALUES FOR CASE 2

During-fault		Post-fault	
$P_{cdf}(pu)$	-0.1012	$P_{caf}(pu)$	-0.0458
$P_{maxdf}(pu)$	0.1059	$P_{maxaf}(pu)$	0.1591
$\gamma_{df}(radian)$	0.0601	$\gamma_{af}(radian)$	0.1383
CCT(s)		0.3679	

TABLE V
SUMMARY OF RESULTS USING THE STATE-PLANE TECHNIQUE

Case No.	Fault duration (cycle)	Fault duration (s)	Detection time(s)	Decision
Case 1	6	0.1000	0.2400	Stable
	8	0.1330	0.2650	Stable
	18	0.3000	0.3700	Unstable
	20	0.3330	0.3950	Unstable
Case 2	8	0.1330	0.2600	Stable
	24	0.4000	0.4700	Unstable
	26	0.4330	0.5040	Unstable

is a stable swing and is detected at 1.9320 s, whereas the detection time for SPA is only 0.2400 s. For Case 1 and fault applied for 18 cycles, the apparent impedance seen by the distance relay is shown in Fig. 19. Since the impedance locus enters the inner blinder, the swing is an unstable swing and is detected as an unstable swing at 0.9470 s whereas the detection time for SPA is only 0.3700 s.

Table VI shows the test results for stable and unstable swings using the two blinder scheme.

VI. CONCLUSION

This paper proposed a novel technique based on SPA to detect first swing out-of-step conditions in two-area power system configurations. The proposed technique is computationally simple and fast compared to the two blinder method. The main advantage of the proposed technique is that it provides a fast prediction of loss of synchronism condition and provides enough time for decision making before the machines actually start slipping poles, thereby preventing unwanted loss of generation and loads. It will also lessen circuit breaker wear and tear as the tripping can be done at a lower voltage angle separation. With the current availability of wide-area measurement systems (WAMS) and phasor measurement units (PMUs) in power systems, the proposed relaying algorithms could be used on large power system configurations. The practical implementation and verification of the proposed algorithm using hardware-in-the-loop simulations would be reported in a future publication.

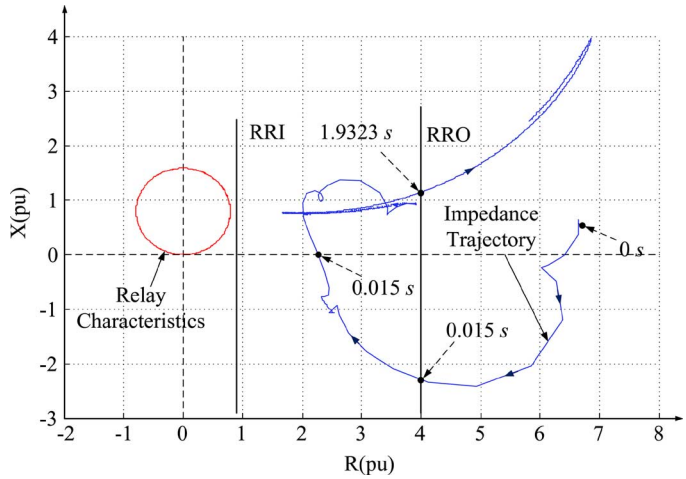

Fig. 18. Impedance trajectory for Case 1 and fault duration of six cycles.

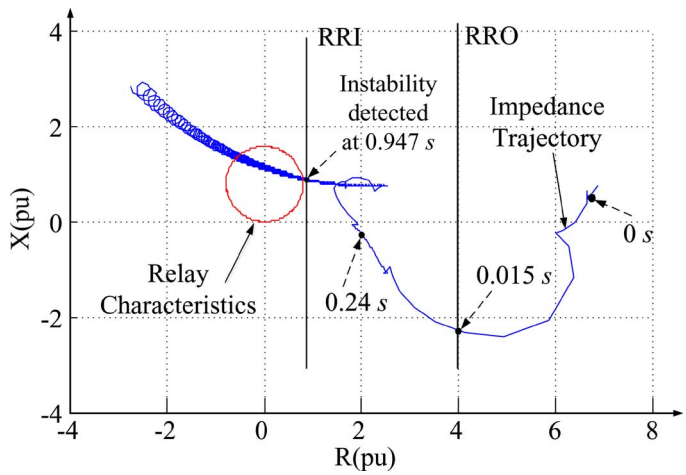

Fig. 19. Impedance trajectory for Case 1 and fault duration of 18 cycles.

TABLE VI
SUMMARY OF RESULTS USING THE TWO BLINDER TECHNIQUE

Case No.	Fault duration (cycle)	Fault duration (s)	Detection time(s)	Decision
Case 1	6	0.1000	1.9323	Stable
	8	0.1330	1.9010	Stable
	18	0.3000	0.9470	Unstable
	20	0.3330	0.8600	Unstable
Case 2	8	0.1330	1.8610	Stable
	24	0.4000	0.9730	Unstable
	26	0.4330	0.9120	Unstable

APPENDIX

SMIB Parameters: Generator rating = 2220 MVA, Base kV = 24 kV

Direct axis transient reactance $(x'_d) = 0.3$ p.u.

Inertia constant $(H) = 3.5$ s, Frequency $= 60$ Hz.

$X_T = j0.15$ p.u., $TL - I = j0.5$ p.u., $TL - II = j1.0$ p.u.

Infinite bus voltage $= 0.9$ p.u.

Two-Area Test System: Generator Data: 900 MVA, 20 kV, $r_a = 0.00125$ p.u., $x_l = 0.2$ p.u., $x_d = 1.8$ p.u., $x_q = 1.76$ p.u., $x'_d = 0.3$ p.u., $x'_q = 0.65$ p.u., $x''_d = 0.25$ p.u., $x''_q = 0.25$ p.u., $T'_{d0} = 8$ s, $T''_{d0} = 0.03$ s, $T'_{q0} = 0.4$ s, $T''_{q0} = 0.05$ s, $H(\mathrm{Gen1}) = 5.4$ s, $H(\mathrm{Gen2}) = 6.25$ s.

Transmission-Line Data: $X_L = 0.53\ \Omega$/km, line lengths: TL-I $= 220$ km, TL-II $= 220$ km, $X_3 = X_4 = 35$ km.

Transformer Data: 900 MVA, 20–230 kV, $X = 0.15$ p.u.

Exciter Data: IEEE-type ST1A exciter, $T_r = 0.01$s, $T_C = 1$ s, $T_B = 10$ s, $K_A = 50$, $V_{\mathrm{MAX}} = 9$ p.u., $V_{\mathrm{MIN}} = -9$ p.u.

Steam Governor Data: GE mechanical-hydraulic controls, Droop $(R) = 0.04$ p.u., speed relay lag time constant (TC) $(T_1) = 0.1$ s, Gate servo TC $(T_3) = 0.25$ s.

Steam Turbine Data (in p.u.): IEEE-type 2 thermal turbine, $K_1 = 0.0$, $K_3 = 0.25$, $K_5 = 0.0$, $K_7 = 0.0$, $K_2 = 0.25$, $K_4 = 0.5$, $K_6 = 0.0$, $K_8 = 0.0$, Steam chest TC $(T_4) = 0.42$ s, Reheater TC $(T_5) = 4.25$ s, reheater/crossover TC $(T_6) = 0.72$ s.

REFERENCES

[1] IEEE Power System Relaying Committee Working Group D6, "Power swing and out-of-step considerations on transmission lines," Jun. 2005.

[2] P. Mooney and N. Fischer, "Application guidelines for power swing detection on transmission systems," presented at the 59th Annu. Conf. Protect. Relay Eng., College Station, TX, 2006.

[3] F. Plumptre, S. Brettschneider, A. Hiebert, M. Thompson, and M. Mynam, "Validation of out-of-step protection with a real time digital simulator," presented at the 60th Annu. Georgia Tech Protect. Relay. Conf., Atlanta, GA, May 2006.

[4] C. Taylor, J. Haner, L. Hill, W. Mittelstadt, and R. Cresap, "A new out-of-step relay with rate of change of apparent resistance augmentation," *IEEE Trans. Power App. Syst.*, vol. PAS-102, no. 3, pp. 631–639, Mar. 1983.

[5] E. Farantatos, R. Huang, G. J. Cokkinides, and A. P. Meliopoulos, "A predictive out of step protection scheme based on pmu enabled dynamic state estimation," presented at the IEEE Power Energy Soc. Gen. Meeting, San Diego, CA, 2011.

[6] W. D. Stevenson, *Elements of Power System Analysis*. New York: McGraw-Hill, 1982.

[7] Y. Xue, T. Van Custem, and M. Ribbens-Pavella, "Extended equal area criterion justifications, generalizations, applications," *IEEE Trans. Power Syst.*, vol. 4, no. 1, pp. 44–52, Feb. 1989.

[8] V. Centeno, A. Phadke, A. Edris, J. Benton, M. Gaudi, and G. Michel, "An adaptive out-of-step relay," *IEEE Trans. Power Del.*, vol. 12, no. 1, pp. 61–71, Jan. 1997.

[9] W. Rebizant and K. Feser, "Fuzzy logic application to out-of-step protection of generators," in *Proc. IEEE Power Eng. Soc. Summer Meet.*, 2001, vol. 2, pp. 927–932.

[10] A. Abdelaziz, M. Irving, M. Mansour, A. El-Arabaty, and A. Nosseir, "Adaptive protection strategies for detecting power system out-of-step conditions using neural networks," *Proc. Inst. Elect. Eng., Gen., Transm. Distrib.* , vol. 145, no. 4, pp. 387–394, Jul. 1998.

[11] A. D. Rajapakse, F. Gomez, K. Nanayakkara, P. A. Crossley, and V. V. Terzija, "Rotor angle instability prediction using post-disturbance voltage trajectories," *IEEE Trans. Power Syst.*, vol. 25, no. 2, pp. 947–956, May 2010.

[12] K. H. So, J. Y. Heo, C. H. Kim, R. K. Aggarwal, and K. B. Song, "Out-of-step detection algorithm using frequency deviation of voltage," *IET Gen., Transm. Distrib.*, vol. 1, no. 1, pp. 119–126, 2007.

[13] L. Wang and A. Girgis, "A new method for power system transient instability detection," *IEEE Trans. Power Del.*, vol. 12, no. 3, pp. 1082–1089, Jul. 1997.

[14] S. Paudyal, G. Ramakrishna, and M. S. Sachdev, "Application of equal area criterion conditions in the time domain for out-of-step protection," *IEEE Trans. Power Del.*, vol. 25, no. 2, pp. 600–609, Apr. 2010.

[15] S. H. Zak, *System and Control*, A. S. Sedra, Ed. New York: Oxford Univ. Press, 2003.

[16] D. R.-V. M. Pavella, M. Pavella, and D. Ernst, *Transient Stability of Power Systems*. Norwell, MA: Kluwer, 2000.

[17] H.-D. Chiang, *Direct Methods for Stability Analysis of Electric Power Systems*. Hoboken, NJ: Wiley, 2011.

[18] J. B. J. Machowski and J. W. Bialek, *Power System Dynamics Stability and Control*. Hoboken, NJ: Wiley, 2008.

[19] E. P. de Souza and A. L. da Silva, "An efficient methodology for coherency-based dynamic equivalents [power system analysis]," *Proc. Inst. Elect. Eng., Gen., Transm. Distrib. C*, vol. 139, no. 5, pp. 371–382, Sep. 1992.

[20] R. Podmore, "Identification of coherent generators for dynamic equivalents," *IEEE Trans. Power App. Syst.*, vol. PAS-97, no. 4, pp. 1344–1354, Jul. 1978.

Binod Shrestha (S'09–M'12) received the B.E. degree in electrical engineering from Tribhuvan University (T.U.), Kathmandu, Nepal, in 2007 and the M.Sc. degree in electrical engineering from the University of Saskatchewan, Saskatoon, SK, Canada, in 2011.

He was with the the University of Saskatchewan. Currently, he is a Grid Planning Engineer (EIT) for Saskatchewan Power Corporation, Regina, SK. His research interests are wide-area power system protection and control, and smart grids.

Ramakrishna Gokaraju (S'88–M'00) received the M.Sc. and Ph.D. degrees in electrical and computer engineering from the University of Calgary, Calgary, AB, Canada, in 1996 and 2000, respectively.

During 1992–94, he was a Graduate Engineer with Larsen & Toubro-ECC, India; a Research Engineer with the Regional Engineering College, Rourkela, India; and a Project Associate with the Indian Institute of Technology, Kanpur, India. From 1999 to 2002, he was a Research Scientist with the Alberta Research Council, Calgary, and a Staff Software Engineer with the IBM Toronto Lab, Toronto, ON, Canada. He joined the University of Saskatchewan, Saskatoon, SK, Canada, in 2003 and is currently an Associate Professor. His current research work is in wide-area power system protection and control, and smart grids.

Mohindar Sachdev (S'63–M'67–SM'73–F'83–LF'97) was born in Amritsar, India, in 1928. He received the B.Sc. degree in electrical engineering from the Banaras Hindu University, Varanasi, India, in 1950, the M.Sc. degree from Punjab University, Chandigarh, India, and the University of Saskatchewan, Saskatoon, SK, Canada, in 1965 and 1967, respectively, and the Ph.D. and D.Sc. degrees from the University of Saskatchewan, Saskatoon, in 1968 and 1994, respectively.

Prof. Sachdev was with the Punjab P.W.D. Electricity Branch and the Punjab State Electricity Board from 1950 to 1968 in system operation, design, and planning. He joined the Electrical Engineering Department, University of Saskatchewan, Saskatoon, SK, Canada, in 1968 and retired from service in 1995. Currently, he is a Professor Emeritus of Electrical Engineering. His area of interest is power system protection.